A continuum-based analytical model for the design of floating energy piles in generalised inhomogeneous soils

A. Della Corte[1], C. Iodice[2], S. François[3], A. Tsikas[4], G. Anoyatis[1*]

[1] *KU Leuven, Department of Civil Engineering, Hydraulics and Geotechnics Section – Bruges, Spoorwegstraat 12, 8200 Bruges, Belgium.*

[2] *University of Campania Luigi Vanvitelli, Department of Engineering, via Roma 29, 81031 Aversa, Italy.*

[3] *KU Leuven, Department of Civil Engineering, Structural Mechanics Section, Kasteelpark Arenberg 40, 3001 Leuven, Belgium.*

[4] *Quantum Neural Technologies (QNT), Patriarchou Ioakeim 34, 10675 Athens, Greece.*

Abstract

This study presents a novel continuum-based semi-analytical framework for the analysis of floating energy piles embedded in generalised inhomogeneous soils. The soil is modelled as an approximate Tajimi-type continuum. Vertical soil inhomogeneity is incorporated into the model by formulating a generalised eigenvalue problem for the evaluation of the soil modes, which are approximated through a series expansion in terms of simple trigonometric functions. The pile and the soil column beneath its tip are represented as a single axially deforming rod, and the restraint effect provided by thermally inactive piles connected to the same cap is accounted for through a concentrated spring at the pile head. In this way, a unified framework in which continuous and piecewise functions, or arbitrary combinations thereof, are used to describe the variation of soil stiffness with depth, is developed to derive the axial force along energy piles. The proposed solution is also extended to include mechanical loads. The predictive capability of the proposed model is assessed through comparisons with established analytical solutions, complex fully coupled numerical analyses and data from full-scale field tests on energy piles supporting a real structure. The very close agreement confirms the reliability of the proposed framework as an efficient alternative to computationally demanding numerical approaches, which can serve as a simple tool for pile design.

Keywords: energy piles; continuum analytical model; pile design; generalised soil inhomogeneity

1 NOTATION

A_p pile cross-sectional area
B_m Fourier coefficients
$E(z)$ pile-soil rod Young's modulus

$E^{'}(z)$ first derivative of $E(z)$
E_{p} pile Young's modulus
$E_{\mathrm{s}}(z)$ depth-dependent soil Young's modulus
$G_{\mathrm{s}0}$ soil shear modulus at the ground surface ($z = 0$)
$G_{\mathrm{s}L/2}$ soil shear modulus at the depth of half pile length ($z = L/2$)
$G_{\mathrm{s}}(z)$ depth-dependent soil shear modulus
G_{si} shear modulus of the i-th soil layer
$H()$ Heaviside step function
K_0 modified Bessel function of zero order and second kind
K_1 modified Bessel function of first order and second kind
K_{h} pile head spring stiffness
L pile length
$N(z)$ axial force acting along the pile-soil rod
$dN(z)/dz$ first derivative of $N(z)$
N_{layers} total number of horizontal soil layers
N_{max} maximum thermally induced axial load
N_{s} total number of sinusoidal functions
N_{t} total number of modes used in the series expansions
P pile head load
R_{km} $N_{\mathrm{t}} \times N_{\mathrm{t}}$ matrix
S_j^m Fourier coefficients for the soil modes approximation

a_j parameters defining the sinusoidal basis functions
b inhomogeneity parameter
d pile diameter
h thickness of the soil deposit
h_{i-1}, h_i depth of the interface between consecutive soil layers
n inhomogeneity parameter
q_m argument of the Bessel functions
r radial coordinate
s_m dimensionless argument of the Bessel functions
u_r radial soil displacement
$u_z = u_z(r, z)$ vertical soil displacement
$\mathrm{w}(z)$ vertical displacement of the pile-soil rod
$d\mathrm{w}(z)/dz$ first derivative of $\mathrm{w}(z)$
z vertical coordinate

α coefficient of the thermal expansion of the pile material
$\delta()$ Dirac delta distribution
δ_{km} Kronecker delta
η_{s} soil compressibility parameter
λ_m m-th eigenvalue

ν_s soil Poisson's ratio
$\Phi_m(z)$ m-th soil mode
$\Phi_m(0)$ m-th soil mode evaluated at the pile head level
$\Phi_m(h)$ m-th soil mode evaluated at the base of the soil deposit
$\Phi_m^{'}(z)$ first derivative of the m-th soil mode
$\Phi_k(z)$ k-th soil mode
$\Phi_k(0)$ k-th soil mode evaluated at the pile head level
$\Phi_k(L)$ k-th soil mode evaluated at the level of the pile tip
$\Phi_k(h)$ k-th soil mode evaluated at the base of the soil deposit
$\Psi(z)$ sinusoidal basis functions
$\Psi^{'}(z)$ first derivative of sinusoidal basis functions
σ_z vertical normal stress in the soil
$\tau_{rz}(r,z)$ vertical shear stress in the soil
$\tau_0(z)$ vertical shear stress at the soil-pile interface
Θ_h normalised pile head spring stiffness
ΔT uniform temperature change in the pile

2 INTRODUCTION

Pile foundations are generally subjected to axial solicitations, which can be due, e.g., to the dead loads transferred from the overlaying building and to the thermal exchange between some piles and the surrounding soil (e.g., Brandl(2006)). While assessing pile response under conventional superstructure loads is engineering practice, estimating the effect of temperature variations on their performance is a less consolidated and more challenging task. This has been exacerbated by the lack of easy-to-use design tools to employ in routine engineering.

Recently, some analytical solutions have been developed for energy piles embedded in multilayer soil. Iodice et al.(2020) used a Winkler-type model and furnished simple expressions to be employed in geotechnical and structural design, along with spring stiffness coefficients calibrated through numerical analyses. They also suggested some rules for the selection of effective soil shear moduli to use in these solutions to account for nonlinear soil behaviour, as well as for the spring stiffness at the pile head to simulate a certain degree of restraint (Iodice et al.(2023)). Other Winkler-type models are also available in literature (Knellwolf et al.(2011), Perić et al.(2020), Olia & Perić(2021), Najma and Sharma(2021), Lyu et al.(2026)), some of which anyhow are developed in an elastic framework.

On one side, these models are usually very simple to implement and are already commonly employed for purely mechanical loads; on the other side, whatever the loading type, they always require a proper selection of the spring stiffness which can be derived by mean of theoretical, experimental or empirical approaches (e.g., Mylonakis(2001), Salgado et al.(2013)). As a result, their predictive capabilities can be undermined by inadequate modeling of soil stiffness through springs, especially in case of inhomogeneous soil.

Continuum-based analytical and semi-analytical approaches are capable to inherently account for the three-dimensional nature of the soil–pile interaction mechanism without requiring

ad hoc calibration of spring constants. In this context, Tajimi-type formulations already developed for piles and walls under mechanical loads Tajimi(1969),Nogami & Novák(1976),Veletsos and Younan(1994), Mylonakis(2001), Anoyatis(2013), Anoyatis et al.(2019), Anoyatis et al.(2023), Della Corte et al.(2025), Della Corte et al.(2026a), Della Corte et al.(2026b), Della Corte et al.(2026c)) can be simply modified to incorporate thermally-induced solicitations. A first attempt was carried out by Iodice & Anoyatis(2024) who used a Tajimi-type model to study the case of end-bearing piles subjected to temperature variations, embedded in homogeneous deposits and in soil characterized by a linear increase of stiffness with depth. This work has been recently extended by Della Corte et al.(2026d) to floating piles specifically for homogeneous soil.

On the same fashion, other continuum-based solutions are available in literature. Huang et al.(2025) presented a three-dimensional analytical model for the thermo-mechanical response of a single end-bearing energy pile embedded in homogeneous soils, which, however involves considerable mathematical complexity and implementation effort due to its three-dimensional framework. Paul and Basu(2026) developed an analytical model for a single energy pile embedded in multilayer soils. A novelty of this work is that soil temperature change is incorporated in the model.

Despite these advantages, there are still several aspects not covered by the few continuum-based analytical solutions available in literature. Among the others, soil inhomogeneity is restricted to a handful of cases, they are developed for free-head energy piles and the possible effect of soil nonlinear behaviour is not considered. To fill these gaps, this paper presents a novel semi-analytical continuum-based framework for the analysis of floating energy piles embedded in inhomogeneous soils, allowing for continuous and piecewise functions, or arbitrary combinations thereof, to describe the variation of soil stiffness with depth. The energy pile is provided with a spring at its head to simulate a certain degree of restraint due to the presence of thermally inactive piles connected to the same rigid cap. Note that the calibration of this spring is conceptually different from that of a Winkler-type model. Indeed, it can be simply derived employing equilibrium and compatibility equations following Iodice et al.(2023).

The soil is considered as a heat reservoir at constant temperature; neglecting the effect of soil temperature change on the thermomechanical response of the pile is a reasonable assumption (Iodice et al.(2020b),Iodice et al.(2023),Paul and Basu(2026)). It is modelled as an approximate Tajimi-type continuum, reducing the two governing elastic equations for an axisymmetric problem to a single equilibrium equation in the vertical direction (Mylonakis(2001), Anoyatis et al.(2019)). The soil column under the pile tip is treated as a pseudopile, with properties identical to those of the surrounding soil. Both the actual and the pseudo-pile segments are modelled as a single axially deforming rod (Anoyatis(2013), Liu and Liu(2024), Della Corte et al.(2026c)). The solution is expressed as a linear combination of soil modes along the vertical coordinate, and vertical soil inhomogeneity is incorporated into the model through the formulation of a generalised eigenvalue problem for the evaluation of the soil modes. These modes are approximated through a series expansion in terms of simple trigonometric functions. Note that although the soil is considered to behave as elastic, nonlinearity is simply accounted for by reducing the small-strain stiffness according to Iodice et al.(2023).

The so-derived solution is then extended to include mechanical loads. This is done exploiting

the principle of superposition, employing the semi-analytical solution derived by Della Corte et al.(2026c) for axially loaded floating piles embedded in generalized inhomogeneous soil.

The main novelties of this work are: establishing a unified framework for floating energy piles that allows to describe any variation of soil stiffness with depth; introducing pile-head restraint by means of a spring connected at its head; developing a unique semi-analytical approach to derive the thermo-mechanical axial force along energy piles subjected to simultaneous mechanical and thermal loads; considering soil nonlinearity drawing upon existing literature.

The predictive capability of the proposed model is assessed through comparisons with established analytical solutions, complex fully coupled numerical analyses and data from full-scale field tests on energy piles supporting a real structure. The comparisons revealed excellent agreement. The effect of selected soil inhomogeneity on the thermally induced axial load is also investigated by means of a parametric study.

Approximate continuum approaches represent an attractive alternative in pile design, since they retain the essential features of the three-dimensional soil–pile interaction while allowing for a simpler mathematical treatment, avoiding parameter calibration as required in case of Winkler-type models. This framework provides a basis for future developments, including the extension to pile-to pile interaction for energy pile groups (e.g., Rotta Loria and Laloui(2016),de Silva et al.(2025)).

3 PROBLEM CONSIDERED

The proposed model first addresses the case of a single floating energy pile subjected to a constant temperature change, ΔT (Figure 1). The pile has length L and diameter d, and is embedded in an inhomogeneous elastic soil layer of thickness h that rests on a rigid base. Soil inhomogeneity is incorporated through a depth-dependent soil shear modulus, $G_{\mathrm{s}}(z)$, which can be described by continuous and piecewise functions, or arbitrary combinations thereof.

In case of continuously inhomogeneous soils, the following generalised power-law function is employed:

$$G_{\mathrm{s}}(z) = G_{\mathrm{s}L/2} \left[b + (1-b) \left(\frac{z}{L/2} \right) \right]^{n} \tag{1}$$

where z is the vertical coordinate (defined positive downward from the ground surface), $G_{\mathrm{s}L/2}$ is the soil shear modulus at $z = L/2$, and n and b are dimensionless inhomogeneity parameters with $b = \left(G_{\mathrm{s}0}/G_{\mathrm{s}L/2}\right)^{1/n}$, where $G_{\mathrm{s}0}$ is the soil shear modulus at $z = 0$. Equation (1) can reproduce a wide range of soil profiles commonly encountered in practice. For example, $n = 1$ and $b = 1$ yields the case of a homogeneous medium, as for heavily overconsolidated clay; while $n = 1$ and $b = 0$ returns a Gibson-type profile with zero stiffness at soil surface. Moreover, using $n = 1$ gives a linear increase of stiffness with depth, which is generally adequate for soft cohesive soils, whereas cohesionless soils are usually well described by a less-than-linear distribution of shear modulus with depth, which can be obtained setting $n = 0.5$ (Di Laora & Rovithis(2015),Anoyatis et al.(2019)).

For the case of layered soils, the variation of soil stiffness is conveniently expressed using the

Heaviside step function, $H()$:

$$G_{\mathrm{s}} = \sum_{i=1}^{N_{\mathrm{layers}}} G_{si} \left[H(z - h_{i-1}) - H(z - h_i) \right] \tag{2}$$

where N_{layers} is the total number of horizontal soil layers, G_{si} is the shear modulus of the i-th layer, and h_{i-1} and h_i denote the depth of the interface between layers $i-1$ and i, and layers i and $i+1$, respectively, with $h_0 = 0$ and $h_{N_{\mathrm{layers}}} = h$.

The soil medium has a constant temperature and is modelled as an approximate continuum of Tajimi-type accounting solely for the effect of the vertical soil displacement component, u_z, on the normal, σ_z, and shear, τ_{rz}, stresses while the influence of the radial displacement, u_r, is considered to be negligibly small (Mylonakis(2001), Anoyatis and Mylonakis(2012), Anoyatis(2013),Della Corte et al.(2026c)). The pile has Young's modulus E_{p} and its head is connected to a concentrated spring of stiffness K_{h} to simulate the restraining action exerted by thermally inactive piles connected to the same rigid cap.

Both the actual pile and the soil column under its tip (pseudo-pile) are modelled as a single axially deforming rod of constant cross-sectional area, A_{p}, and Young's modulus expressed as follows (Anoyatis(2013), Liu and Liu(2024), Della Corte et al.(2026c)):

$$E(z) = E_{\mathrm{p}} + \left(E_{\mathrm{s}}(z) - E_{\mathrm{p}} \right) H(z - L) \tag{3}$$

where $E_{\mathrm{s}}(z)$ is the Young's modulus of the soil. The latter can be derived from $G_{\mathrm{s}}(z)$ considering that a constant Poisson's ratio, ν_{s}, is assumed throughout the soil thickness. According to equation (3), the section of the rod representing the soil underneath pile tip has stiffness $E_{\mathrm{s}}(z)$.

Perfect contact (i.e., neither gap nor slippage) is assumed at the soil-pile interface.

4 MODEL DEVELOPMENT

In the following, the analysis will first focus on the soil medium and then on the pile-soil interaction.

4.1 Soil analysis

For a Tajimi-type continuum, the equilibrium of a soil element along the vertical direction in axisymmetric conditions returns the following second-order homogeneous partial differential equation (Anoyatis et al.(2019)):

$$G_{\mathrm{s}}(z) \frac{1}{r} \frac{\partial}{\partial r} \left(r \frac{\partial u_z}{\partial r} \right) + \eta_{\mathrm{s}}^2 \frac{\partial}{\partial z} \left(G_{\mathrm{s}}(z) \frac{\partial u_z}{\partial z} \right) = 0 \tag{4}$$

where $u_z = u_z(r, z)$ is the vertical soil displacement in cylindrical coordinates, i.e., the unknown of the problem, and $\eta_s^2 = 2/(1 - \nu_{\mathrm{s}})$ is a compressibility parameter related to the Tajimi approximation (Mylonakis(2001), Anoyatis et al.(2019)).

The solution of equation (4) can be obtained by applying the method of separation of

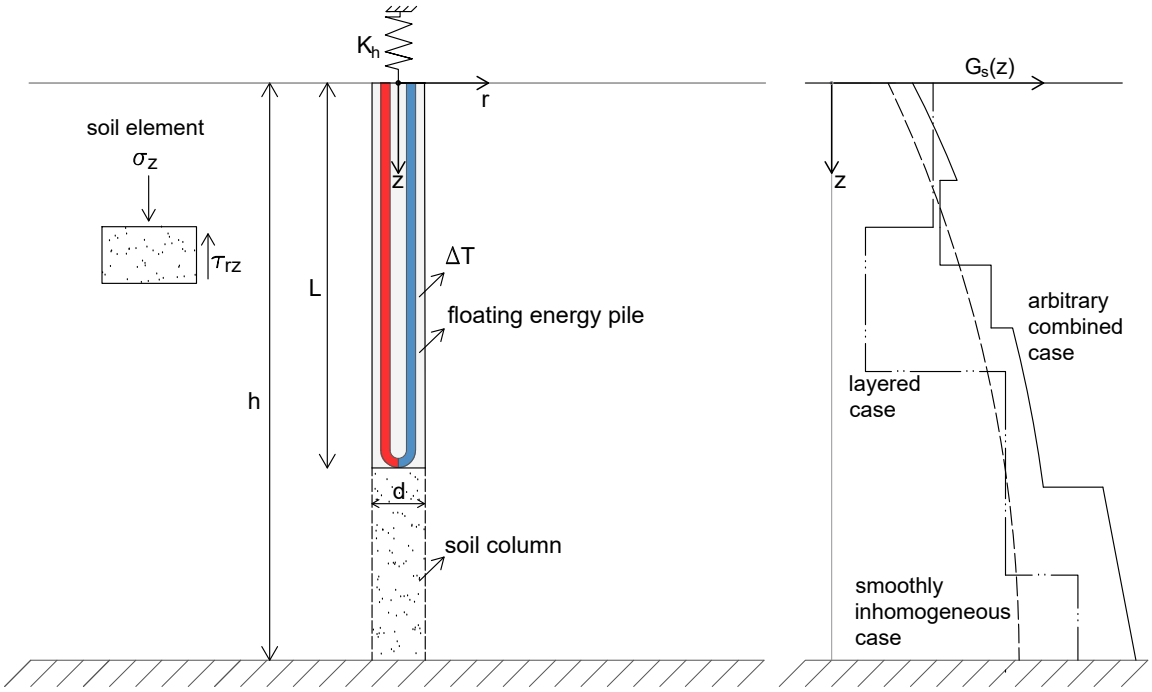


Figure 1: Schematic representation of the problem considered.

variables. By imposing

$$u_z(r,z) = R\,(r)\,\Phi\,(z) \tag{5}$$

the following two ordinary differential equations are obtained (Anoyatis(2013)):

$$R''(r) \,+\, \frac{1}{r}R'(r) \,-\, q^2 R(r) \,=\, 0 \tag{6}$$

and

$$\big(G_{\rm s}(z)\,\Phi'(z)\big)' \,+\, \lambda\, G_{\rm s}(z)\,\Phi(z) \,=\, 0 \tag{7}$$

in which λ are the eigenvalues and $\Phi(z)$ are the corresponding eigenfunctions (soil modes) of the Sturm–Liouville (SL) problem, with $\Phi'(z)$ being the first derivative of the soil modes, and $q = \eta_{\rm s}\sqrt{\lambda}$.

It is noted that equation (6) is a linear second-order ordinary differential equation whose solution was derived by Mylonakis(2001) and Anoyatis et al.(2019). As concerns equation (7), it represents a (SL) problem with variable coefficients. Its exact solution was presented by Anoyatis et al.(2019), while, recently, an approximate expression was derived by Della Corte et al.(2025),Della Corte et al.(2026c) using pertinent generalised Fourier series expansion, extending the application of (SL) theory also to dynamic soil–pile interaction problems (Della Corte et al.(2026b)). The latter is used in the proposed approach. In particular, the soil modes are expressed as follows:

$$\Phi_m(z) \,=\, \sum_{j=1}^{N_{\rm s}} S_j^m\,\Psi_j(z) \tag{8}$$

where S_j^m are Fourier coefficients and $\Psi_j(z)$ are sinusoidal functions:

$$\Psi_j(z) \;=\; \cos(a_j z) \tag{9}$$

with $a_j = (\pi/2h)(2j-1)$ and $j = 1, 2, 3, \ldots N_\mathrm{s}$, where N_s is the total number of sinusoidal functions considered in the series expansion. The Fourier coefficients can be obtained from equations (7) and (8), integrating along the thickness of the soil layer and enforcing two boundary conditions, one at the base of the soil layer, where $\Phi_m(h) = 0$ (zero displacement), and the other at soil surface, where $\Phi'_m(0) = 0$ (zero normal stress). This way, the following expression is derived:

$$\sum_{j=1}^{N_\mathrm{s}} S_j^m \left(\int_0^h G_\mathrm{s}(z)\, \Psi_j^{'}(z)\, \Psi_k^{'}(z)\, dz \right) \;-\; \sum_{j=1}^{N_\mathrm{s}} S_j^m\, \lambda_m \left(\int_0^h G_\mathrm{s}(z) \Psi_j(z) \Psi_k(z)\, dz \right) \;=\; 0 \tag{10}$$

Once the eigenvalue problem is solved, the displacements and shear stresses in the soil can be derived using the following expressions:

$$u_z(r,z) = \sum_{m=1}^{N_\mathrm{t}} B_m\, K_0(q_m r)\, \Phi_m(z) \tag{11}$$

and

$$\tau_{rz}(r,z) = -G_\mathrm{s}(z) \frac{du_z(r,z)}{dr} = G_\mathrm{s}(z) \sum_{m=1}^{N_\mathrm{t}} B_m\, q_m\, K_1(q_m r)\, \Phi_m(z) \tag{12}$$

where N_t is the total number of modes used in the series expansion, and $K_0(\cdot)$ and $K_1(\cdot)$ are the modified Bessel functions of the second kind, of zero and first order, respectively. B_m are the unknown Fourier coefficients, which will be determined in the next section (soil-pile interaction analysis) by enforcing perfect contact at the soil-pile interface.

4.2 Soil-pile interaction analysis

When a pile is subjected to a temperature variation it experiences elongation or shortening due to heating or cooling, respectively. The magnitude of thermally-induced axial strains depends on the restraining action exerted on the pile by the soil along the shaft and underneath its base, and by other piles connected to the same cap. As a consequence, a thermally-induced axial force develops, $N(z)$, which for the elastic pile-soil rod in the proposed model can be expressed as follows (Della Corte et al.(2026d)):

$$N(z) = E(z) A_\mathrm{p} \left(\alpha \Delta T H(L-z) - \frac{d\mathrm{w}(z)}{dz} \right) \tag{13}$$

where α is the coefficient of the thermal expansion of the pile material (here expansion is considered positive) and $\mathrm{w}(z)$ is the vertical displacement of the pile-soil rod which is the unknown of the problem. The first term in brackets represents the thermal strain that the pile would be subject to if free to displace, while the second is the strain which actually develops due to the imposed temperature variation. Note that the soil column under pile tip doesn't experience any temperature variation; it undergoes mechanical deformation induced by pile

elongation or shortening.

The equilibrium of vertical forces acting on a pile-soil rod segment yields the following governing equation:

$$\frac{dN(z)}{dz} + \pi d\tau_0(z) = 0 \tag{14}$$

where $\tau_0(z) = \tau_{rz}(d/2, z)$ is the vertical shear stress at the soil-pile interface which can be calculated using equation (12).

Substituting equation (13) into the above equilibrium equation, one obtains:

$$\begin{aligned} &- E(z)A_\mathrm{p}\frac{d^2\mathrm{w}(z)}{dz^2} - E'(z)A_\mathrm{p}\frac{d\mathrm{w}(z)}{dz} + \pi d\,\tau_0(z) \\ &= E(z)A_\mathrm{p}\,\alpha\Delta T\,\delta(L-z) - E'(z)A_\mathrm{p}\,\alpha\Delta T\,H(L-z) \end{aligned} \tag{15}$$

where $E'(z)$ stands for the first derivative of $E(z)$ with respect to z, and $\delta()$ is the delta Dirac distribution coming from the first derivative of $H()$ with respect to z.

Equation (15) is a second order differential equation and can be solved upon some mathematical manipulations and by enforcing two boundary conditions, one at pile head where the axial force is a function of K_h and the other at the base of the model where $\Phi_k(h) = 0$. In particular, considering perfect contact at the pile-soil interface, i.e., $\mathrm{w}(z) = u_z(d/2, z)$, substituting Equations (11), and (12) into (15), multiplying by $\Phi_k(z)$, and integrating with respect to z in the interval $(0, h)$, one obtains:

$$\begin{aligned} &A_\mathrm{p}\sum_{m=1}^{N_\mathrm{t}} B_m K_0(s_m)\int_0^h E(z)\,\Phi'_m(z)\,\Phi'_k(z)\,dz + K_\mathrm{h}\,\Phi_k(0)\sum_{m=1}^{N_\mathrm{t}} B_m K_0(s_m)\,\Phi_m(0) + \\ &2\pi\,B_k\,s_k\,K_1(s_k)\int_0^h G_\mathrm{s}(z)\,\Phi_k^2(z)\,dz = E_\mathrm{p}A_\mathrm{p}\,\alpha\Delta T\,(\Phi_k(L) - \Phi_k(0)) \end{aligned} \tag{16}$$

where $s_m = q_m\,d/2$ is the dimensionless argument of the Bessel function $K()$. Equation (16) can be rearranged in matrix form as follows:

$$\left[R_{km}\right]\{B_m\} = E_\mathrm{p}A_\mathrm{p}\,\alpha\Delta T\,\{\Phi_k(L) - \Phi_k(0)\} \tag{17}$$

where R_{km} is an $N_\mathrm{t} \times N_\mathrm{t}$ matrix:

$$\begin{aligned} R_{km} = {} & A_\mathrm{p}K_0(s_m)\left(\int_0^h E(z)\,\Phi'_m(z)\,\Phi'_k(z)\,dz\right) + K_\mathrm{h}\,\Phi_k(0)\,\Phi_m(0)\,K_0(s_m) + \\ & \left[2\pi\,s_k\,K_1(s_k)\left(\int_0^h G_\mathrm{s}(z)\,\Phi_k^2(z)\,dz\right)\right]\delta_{km} \end{aligned} \tag{18}$$

and the terms related to Kronecker delta contribute only to the diagonal terms of the matrix (i.e., $\delta_{km} = 0$ for $m \neq k$ and $\delta_{km} = 1$ for $m = k$) as determined by the orthogonality property of the soil modes (Anoyatis(2013), Anoyatis et al.(2019)).

Thus, the displacement and the shear stress of the soil-pile rod are obtained as follows:

$$\mathrm{w}(z) = \sum_{m=1}^{N_\mathrm{t}} B_m K_0(s_m)\Phi_m(z) \tag{19}$$

$$\tau_0(z) = G_{\mathrm{s}}(z) \sum_{m=1}^{N_{\mathrm{t}}} B_m \, q_m \, K_1(s_m) \, \Phi_m(z) \tag{20}$$

where the coefficients B_m are calculated using equation (17).

Then thermally induced axial force on the pile-soil rod, $N(z)$, is determined numerically by means of equations (14) and (20).

Beyond pile geometry and stiffness, the proposed solution only requires a handful of ingredients, which are the soil stiffness and soil Poisson's ratio, and the stiffness of the spring at pile head.

5 MODEL VERIFICATION AND VALIDATION

5.1 Influence of the total number of modes N_{t}

Since the proposed solution is expressed as a linear combination of soil modes along the vertical coordinate, a convergence analysis is performed with respect to the total number of modes, N_{t}. Figure 2 shows the influence of N_{t} on the normalised maximum thermal load, $N_{\max} \,/\, \alpha \Delta T E_{\mathrm{p}} A_{\mathrm{p}}$, for selected pile slenderness ratios, L/d, and two pile-soil stiffness ratios, namely (a) and (c) $E_{\mathrm{p}}/G_{\mathrm{s}L/2} = 100$ and (b) and (d) $E_{\mathrm{p}}/G_{\mathrm{s}L/2} = 5000$. Two soil stiffness profiles are considered: homogeneous soils (grey lines) and a soil with a linear variation of stiffness with depth and zero stiffness at the surface (black lines). The soil layer has a dimensionless thickness of $h/L = 2$, while its Poisson's coefficient is set to 0.4. The analyses are carried out with reference to both free- and fixed-head piles. This is achieved by choosing appropriate values for the dimensionless head stiffness, $\Theta_{\mathrm{h}} = K_{\mathrm{h}} L \,/\, E_{\mathrm{p}} A_{\mathrm{p}}$. In particular, $\Theta_{\mathrm{h}} = 0$ and $\Theta_{\mathrm{h}} = 10^5$ are used for free- and fixed-head conditions, respectively. Note that the latter value is the result of a sensitivity analysis showing that practically fully restrained conditions are already attained for $\Theta_{\mathrm{h}} \geq 10^4$.

It is evident that sufficient convergence of the solution is achieved for $N_{\mathrm{t}} \geq 80$. Therefore, all subsequent analyses are performed using $N_{\mathrm{t}} = 100$ modes.

5.2 Influence of the soil deposit thickness

The proposed model accounts for the presence of a bedrock at $z = h$. It is noted that the analyses in Figure 2 are carried out for $h/L = 2$ which can be considered as representative of a fully floating pile, as demonstrated in the ensuing.

To investigate the influence of h/L on the normalised maximum thermal load, $N_{\max} \,/\, \alpha \Delta T E_{\mathrm{p}} A_{\mathrm{p}}$, Figure 3 shows the results of some analyses involving different pile slenderness ratios, L/d, and two pile-soil stiffness ratios, namely (a) $E_{\mathrm{p}}/G_{\mathrm{s}L/2} = 100$ and (b) $E_{\mathrm{p}}/G_{\mathrm{s}L/2} = 5000$, considering both homogeneous (grey lines) and inhomogeneous distributions (black lines). The pile has no restraint at its head. As expected, the maximum thermal load decreases as h/L increases, up to approximately $h/L \approx 1.5$, beyond which it becomes essentially insensitive to further increases in layer thickness. This trend reflects the progressive reduction of the influence of the rigid base, and for $h/L \approx 1.5$ the response approaches that of a pile embedded in a half-space.

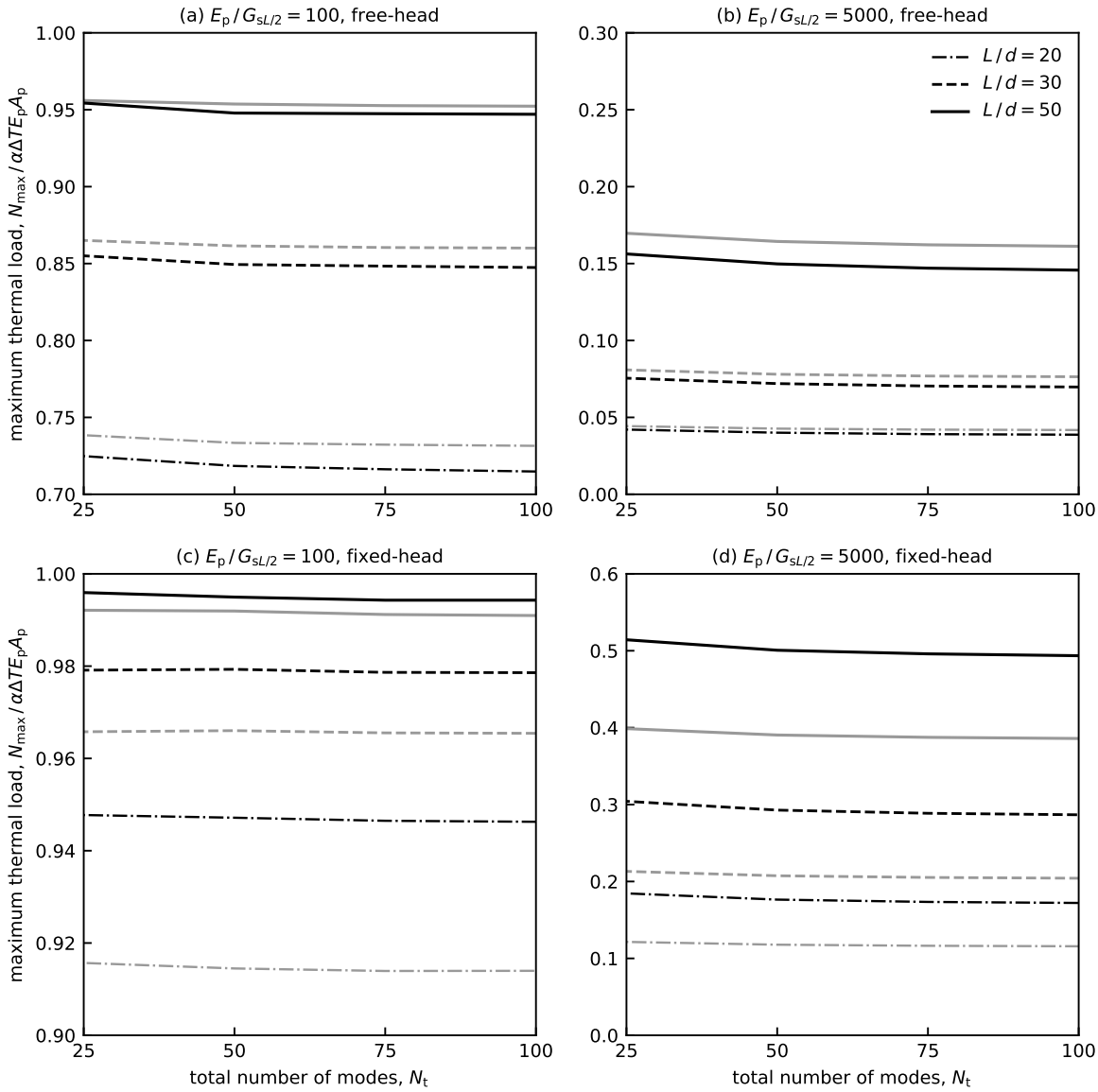


Figure 2: Investigation of the effect of the total number of modes, N_t, on the normalised maximum thermal load, $N_\mathrm{max} \,/\, \alpha \Delta T E_\mathrm{p} A_\mathrm{p}$, for selected pile slenderness ratios, L/d, and two pile-soil stiffness ratios: (a) and (c) $E_\mathrm{p}/G_{\mathrm{s}L/2} = 100$ and (b) and (d) $E_\mathrm{p}/G_{\mathrm{s}L/2} = 5000$. The grey lines refer to homogeneous soils ($n = 1$, $b = 1$ in Eq. (1)), and the black ones to soils with a linear variation of the stiffness with depth and zero stiffness at the surface ($n = 1$, $b = 0$ in Eq. (1)). $h/L = 2$, $\nu_\mathrm{s} = 0.4$.

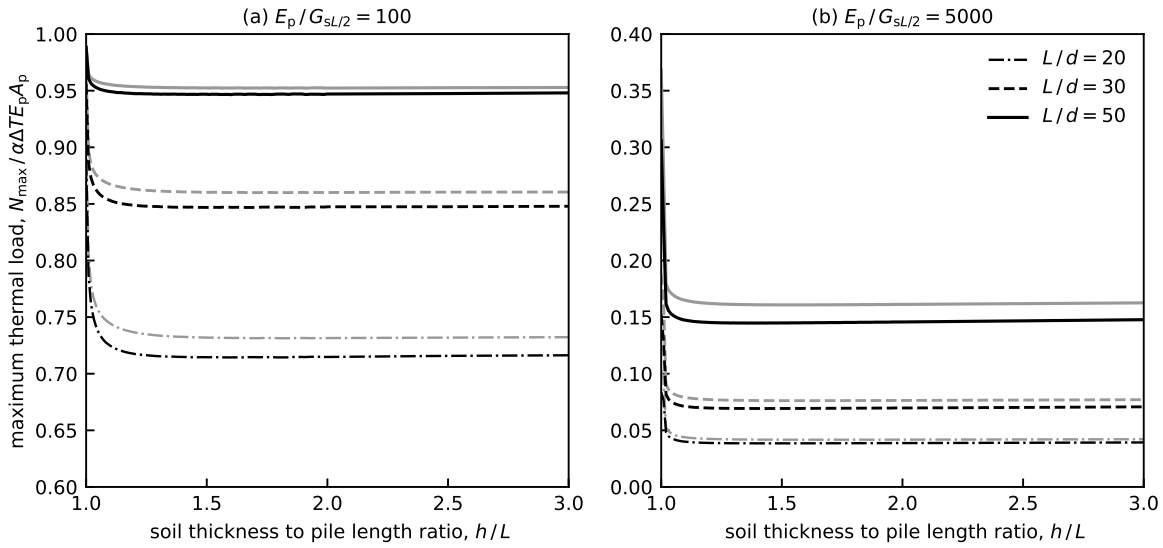


Figure 3: Investigation of the effect of the soil normalised thickness, h/L, on the normalised maximum thermal load, $N_{\max} / \alpha \Delta T E_{\mathrm{p}} A_{\mathrm{p}}$, for selected pile slenderness ratios, L/d, and two pile-soil stiffness ratios: (a) $E_{\mathrm{p}}/G_{\mathrm{s}L/2} = 100$ and (b) $E_{\mathrm{p}}/G_{\mathrm{s}L/2} = 5000$. The grey lines refer to homogeneous soils ($n = 1$, $b = 1$ in Eq. (1)), and the black ones to soils with a linear variation of the stiffness with depth and zero stiffness at the surface ($n = 1$, $b = 0$ in Eq. (1)). $\nu_{\mathrm{s}} = 0.4$, $\Theta_{\mathrm{h}} = 0$ (free-head).

5.3 Validation against analytical solution and numerical analyses

The predictive performance of the proposed model is verified against the Winkler-type analytical solution reported by Iodice et al.(2020), as well as against the results of some linear elastic Finite Element analyses carried out by the same authors.

Figure 4 shows a comparison in terms of normalised thermally induced axial load, $N(z)/\alpha \Delta T E_{\mathrm{p}} A_{\mathrm{p}}$, developed along normalised depth, z/L, for selected L/d and for $E_{\mathrm{p}}/G_{\mathrm{s}L/2} = 1000$. The results refer to a free-head pile embedded in a homogeneous deposit (Figure 4 (a)) and in a deposit characterized by a stiffness profile proportional to depth (Figure 4 (b)). Note that the stiffness of this two distributions is selected such that it matches at $z/L = 0.5$.

Overall, good agreement is observed among the three approaches. In particular, the proposed solution shows a close match with the numerical analyses confirming its predictive capability. The slight overestimation of the dimensionless thermally induced axial load is attributed to the approximate nature of the continuum-based formulation. It can be noted that the normalised thermally induced axial load increases with increasing pile slenderness ratio regardless of soil inhomogeneity. Since the stiffness at pile mid-length is the same, as expected, $N(z)/\alpha \Delta T E_{\mathrm{p}} A_{\mathrm{p}}$ in the upper portion of the pile is largest for homogeneous soil, while the opposite occurs toward pile base. Moreover, the normalized maximum thermally induced axial load is placed at a deeper location in case of stiffness proportional to depth (i.e., the null point is at about $z/L \simeq 0.71$-0.73, Figure 4 (b)) compared to constant stiffness distribution (i.e., the null point is at about $z/L \simeq 0.55$, Figure 4 (a)).

Figure 5 presents the same comparison as Figure 4 for the case of fixed-head energy pile.

A very good agreement is detected, especially for inhomogeneous soil. Anyhow, it is worth noting that when the soil stiffness is constant, the proposed solution shows a local deviation in the vicinity of pile head (Figure 5 (a)). Indeed, while the Winkler-type solution and the FE results attain the maximum axial load at $z = 0$, the distribution derived with the continuum-based approach predicts that the maximum load is located at $z/L \approx 0.18$. This deviation is attributed to the approximate nature of the adopted continuum formulation, which leads to a singularity in the shear stress profile near pile head, resulting in a boundary-layer-type behaviour Anoyatis and Mylonakis(2012). The equilibrium of forces in the radial direction is not satisfied in this approach, nor is the boundary condition of vanishing shear stress at the soil surface Mylonakis(2001). This has an influence on the shear stress distribution (Figure 6), which, in case of fixed-head pile embedded in a soil with constant stiffness, changes sign at $z/L \approx 0.18$ (Figure 6 (b)), producing a local maximum in the axial load through the pile-soil equilibrium relation. Nevertheless, this effect has limited practical significance, as it does not appreciably affect the overall axial load distribution along the pile. For a Gibson soil profile with $G_s(0) = 0$, since the shear stress vanishes at $z = 0$ by definition (Figure 6 (b)), as follows directly from Equation (12) , the near-surface behaviour has much less influence on the axial load distribution, and the proposed solution closely matches the FE results also at ground surface.

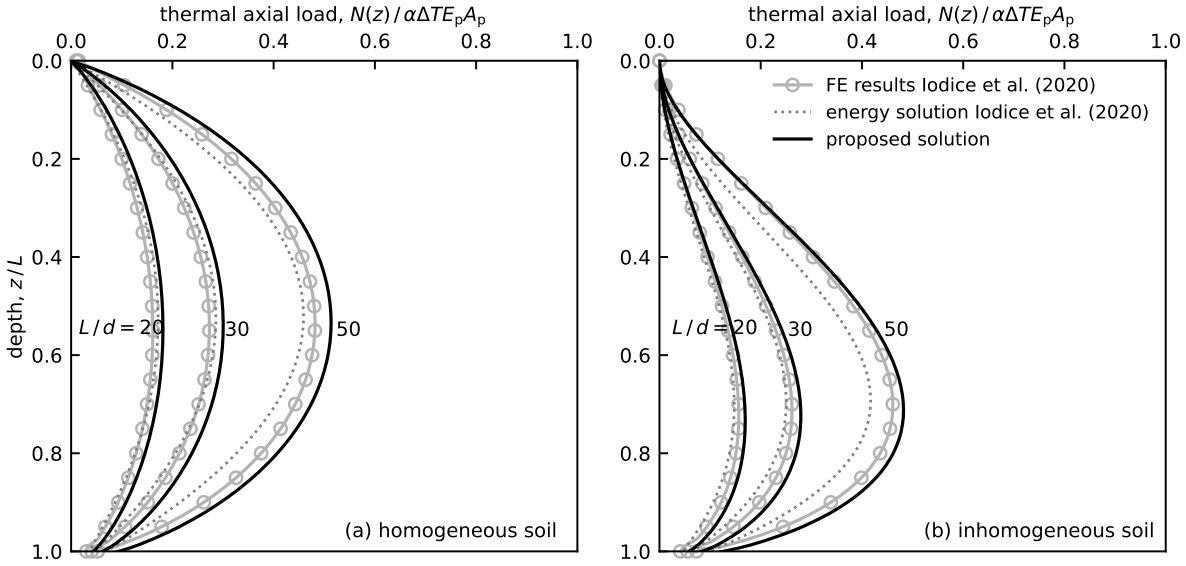


Figure 4: Variation of the normalised thermal axial load, $N(z)\,/\,\alpha\Delta T E_p A_p$, with the normalised depth, z/L, for selected pile slenderness ratios, L/d, and pile-soil stiffness ratio $E_p/G_{sL/2} = 1000$, in case of (a) homogeneous ($n = 1$, $b = 1$ in Eq. (1)) and (b) inhomogeneous soils ($n = 1$, $b = 0$ in Eq. (1)). Comparison of the proposed solution with the finite element results and the energy solution of Iodice et al.(2020). $h/L = 2$, $\nu_s = 0.4$, $\Theta_h = 0$ (free-head).

5.4 Validation against experimental data

To further assess the predictive capability of the proposed model, it has also been validated against some data gathered from field measurements as well as against the results of Finite Element nonlinear analyses.

Two well-documented experimental campaigns are considered, which refer to an isolated

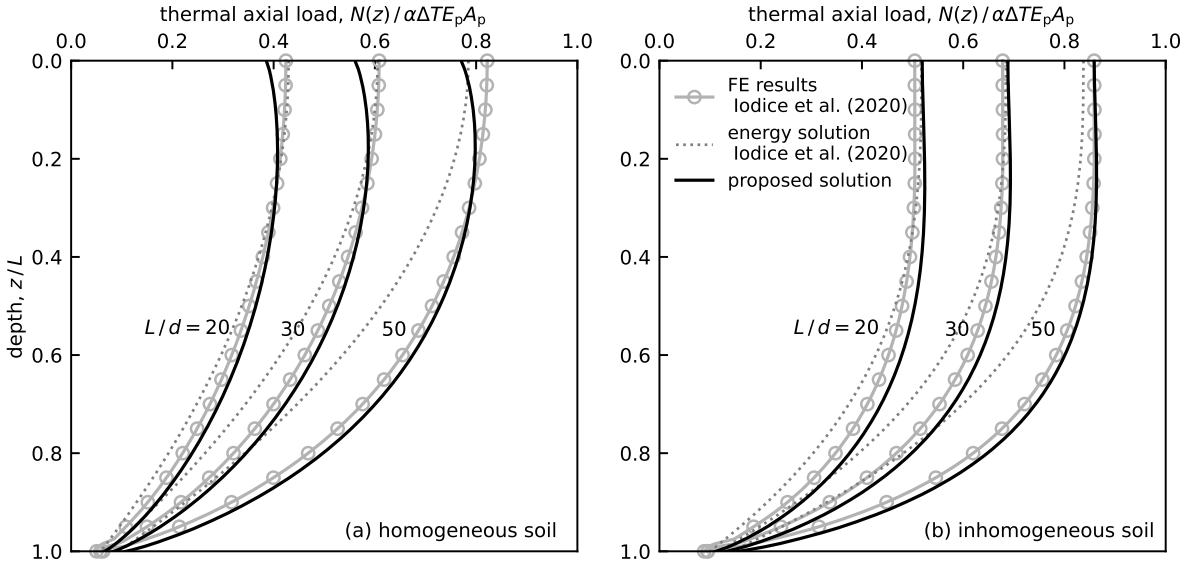


Figure 5: Variation of the normalised thermal axial load, $N(z)\,/\,\alpha\Delta TE_pA_p$, with the normalised depth, z/L, for selected pile slenderness ratios, L/d, and pile-soil stiffness ratio $E_p/G_{sL/2} = 1000$, in case of (a) homogeneous ($n = 1$, $b = 1$ in Eq. (1)) and (b) inhomogeneous soils ($n = 1$, $b = 0$ in Eq. (1)). Comparison of the proposed solution with the finite element results and the energy solution of Iodice et al.(2020). $h/L = 2$, $\nu_s = 0.4$, $\Theta_h = 10^5$ (fixed-head).

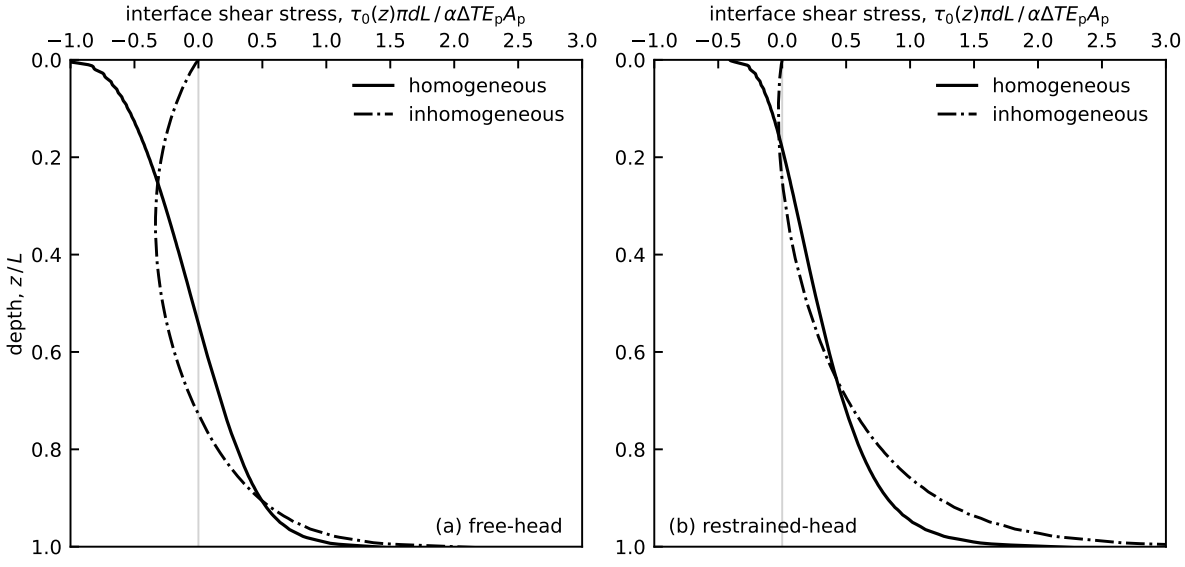


Figure 6: Variation of the normalised interface shear stress, $\tau_0(z)\pi dL\,/\,\alpha\Delta TE_pA_p$, with the normalised depth, z/L, for a homogeneous ($n = 1$, $b = 1$ in Eq. (1)) and inhomogeneous soils ($n = 1$, $b = 0$ in Eq. (1)). (a) free-head ($\Theta_h = 0$), and (b) restrained-head ($\Theta_h = 10^5$). $L/d = 20$, $E_p/G_{sL/2} = 1000$, $h/L = 2$, $\nu_s = 0.4$, $N_t = 250$.

energy pile embedded in a soil with stiffness linearly increasing with depth and to a group of energy piles in a layered deposit, as detailed in the ensuing.

A single pile test carried out at the Lambeth College, London, UK, is reported by Bourne-Webb et al.(2009). It involved a 23 m long pile having a diameter of 0.61 m, up to about 5 m, and of 0.55 m along the remaining length, embedded in a London Clay layer, overlaid by a 4 m stratum of made ground and river terrace deposits. The temperature variation was preceded by the application of a vertical mechanical load at pile head which was kept constant throughout the following tests, at 1200 kN. Thermal testing began from an initial temperature of about 20 °C, and involved pile cooling up to approximately 0 °C, followed by pile heating up to about 30 °C, and by three daily cycles.

The thermally-induced axial force exerted along pile length after the cooling phase is reported in Figure 7. This is derived from the strain recorded during the tests via optical fibre sensors, OFS (Amatya et al.(2012)). In particular, measurements were available after the application of the mechanical load and at the end of the first cooling; the difference between these two sets of measurements represents the second term in brackets of Equation (13). The first term is simply derived from temperature recordings through OFS (Amatya et al.(2012)).

In the proposed approach, the pile is considered to have a constant diameter of 0.55 m, while the small-strain shear modulus of the clay is estimated following Vardanega and Bolton(2011), who proposed $G_s(z) = 320.7\, s_u(z)$ for London clay, where $s_u(z)$ is the soil resistance in undrained condition. Soil and pile properties are adopted from Amatya et al.(2012). Since the test involves an isolated pile, no restraint is considered at pile head.

Figure 7 compares the predictions of the proposed analytical solution with the thermally-induced axial load derived from OFS measurements; the Winkler-type energy solution by Iodice et al.(2020) is also reported for comparison. It can be noted that agreement with the field measurement is excellent.

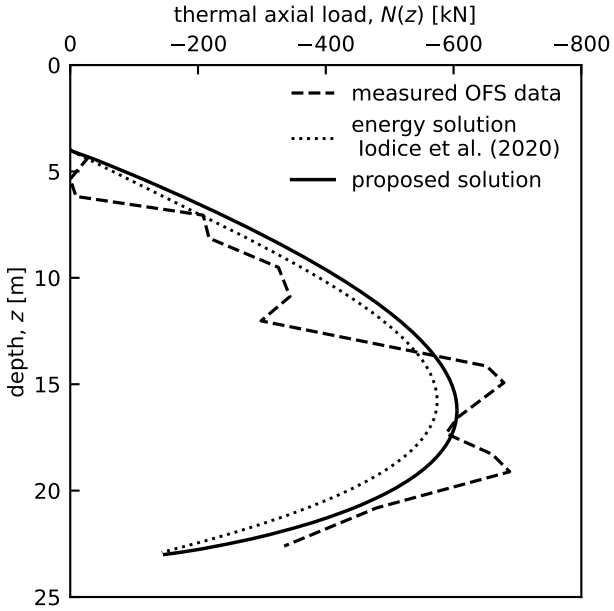


Figure 7: Lambeth College test: Comparison between the field data, the energy solution of Iodice et al.(2020) and the proposed solution.

The other case history concerns the foundation of a water retention tank, which consists of a 0.9 m thick raft supported by 16 conventional piles, 16 m long and 0.6 m in diameter, together with 4 energy piles, EP1-EP4, 28 m long with a diameter of 0.9 m (Mimouni and Laloui(2015), Di Donna et al.(2016), Rotta Loria and Laloui(2018)). A plan view of the foundation is provided in Figure 8. The group is embedded in a layered deposit made of four strata, overlying a stiff bedrock. Note that the top 4 m of each pile is thermally insulated to prevent thermal interaction with the water stored in the tank. Therefore, the energy piles are considered to be 24 m long. Further details about pile layout and instrumentation can be found in the original references.

The thermal testing was carried out during the construction of the tank; thus, piles are subjected to simultaneous thermo-mechanical solicitations. In the following, pile and soil properties, applied loads and the exerted degree of restraint at pile heads are selected following Iodice et al.(2023). In particular, the small strain soil shear modulus has been reduced to consider in a straightforward manner the development of nonlinearities due to the application of the vertical mechanical load. This reduction is expressed through a factor which is evaluated from the load-settlement relationship of the pile, deduced from the data available in the related references. In addition to this, to account for the restraint at pile head, K_{h} has been calibrated by solving a simple system of equilibrium and compatibility equations. This is written by representing the piles as concentrated springs attached to a rigid raft, with a stiffness equal to the axial stiffness of the corresponding piles (Randolph and Wroth(1978)). The active piles are then subjected to a known thermally-induced displacement, equal to that at the head of a free-head pile. The calculations were carried out both considering and neglecting thermal and mechanical pile-to-pile interaction effects (Rotta Loria and Laloui(2016), Randolph and Wroth(1978)). K_{h} is then estimated as the ratio between the load and the settlement experienced by the thermally active pile (Iodice et al.(2023)).

Figure 8 compares the thermally induced axial stress as derived from different tests on the same foundation, with the predictions obtained using the proposed model and the corresponding results by Iodice et al.(2023). In particular, single pile tests were reported by Mimouni and Laloui(2015), Di Donna et al.(2016) and Rotta Loria and Laloui(2018) in which one energy pile is activated at a time; moreover, Rotta Loria and Laloui(2018) also reported the result of a group test in which the 4 energy piles were thermally activated simultaneously (EP1-All in Figure 8).

The results suggest that the proposed semi-analytical solution can capture pile behaviour very well; since the tests involved both single pile and group configurations, the capability of reproducing a certain degree of restraint at pile head is also verified. As expected, the incorporation of thermal and mechanical pile-to-pile interaction leads to a lower thermally-induced axial stress profile.

6 PARAMETRIC ANALYSIS

The effect of different soil shear modulus profiles on the distribution of the normalised thermally induced axial load with normalised depth, is shown in Figure 9, for $L/d = 30$, $E_{\mathrm{p}}/G_{\mathrm{s}L/2} = 1000$, and both free- and fixed-head conditions. In particular, four continuous distributions of soil stiffness with depth are considered, all sharing the same soil shear modulus at $z = L/2$, together with two two-layer soil profiles whose average stiffness is equal to that of the continuous profiles

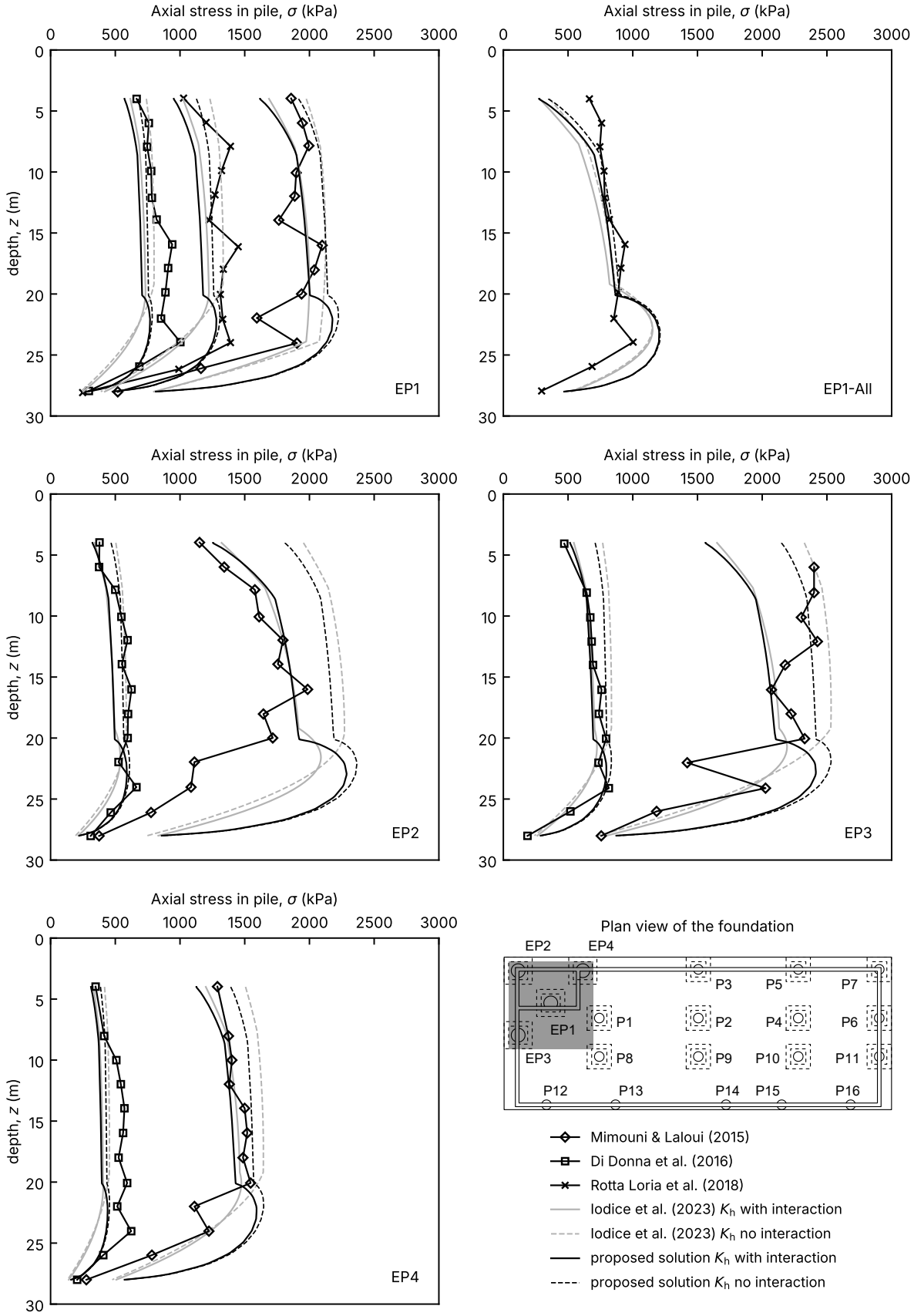


Figure 8: Comparison between the field data (EP1, EP1-All, EP2, EP3 and EP4), the energy solution of Iodice et al.(2023) and the proposed solution.

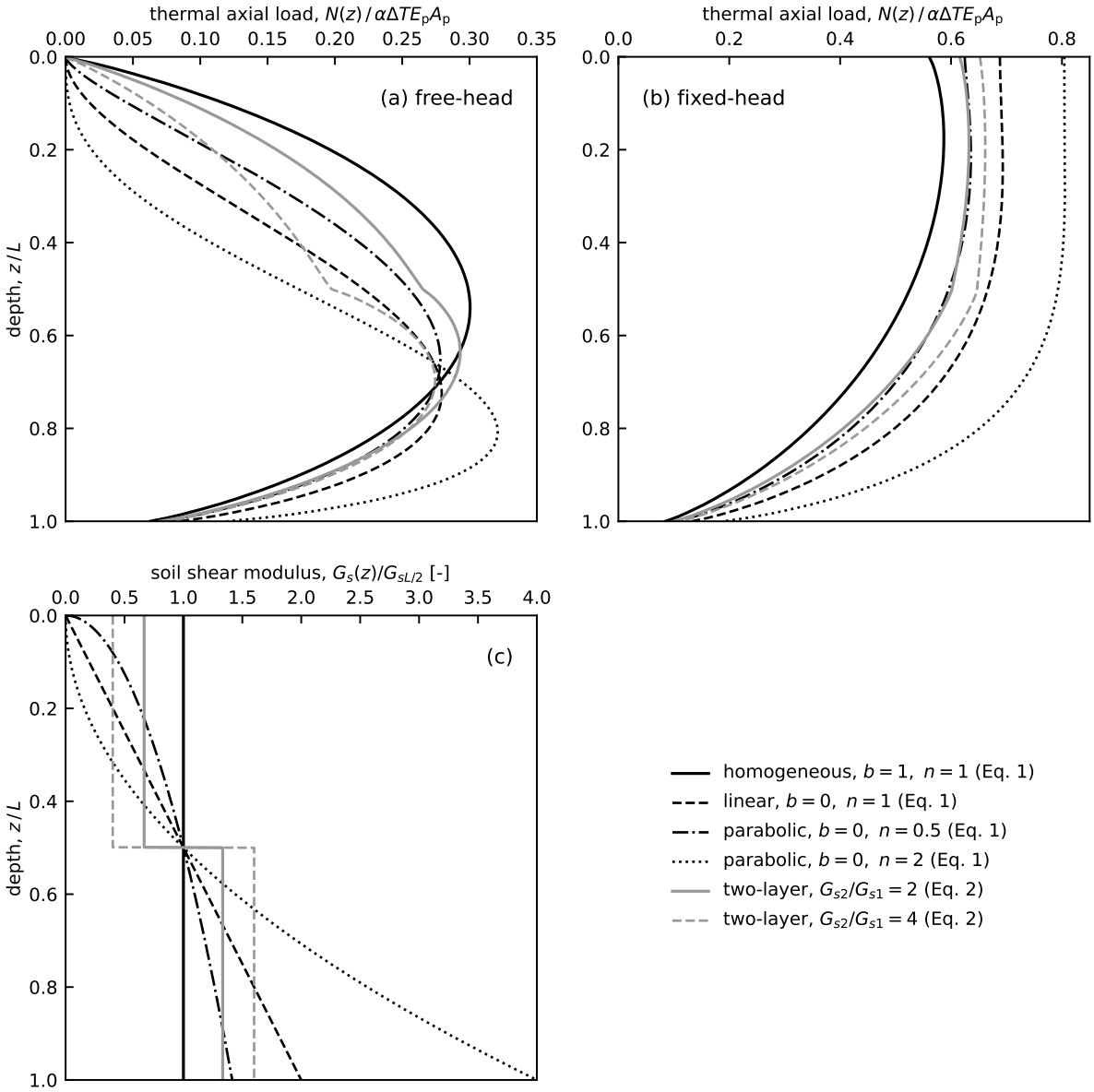


Figure 9: Effect of different soil shear modulus profiles on the distribution of the normalised thermal axial load, $N(z)\,/\,\alpha\Delta T E_\mathrm{p} A_\mathrm{p}$. (a) results for free-head case ($\Theta_\mathrm{h}=0$), (b) fixed-head case ($\Theta_\mathrm{h}=10^5$), (c) normalised soil shear modulus profiles. $h/L=2$, $\nu_\mathrm{s}=0.4$, $E_\mathrm{p}/G_{\mathrm{s}L/2}=1000$, $L/d=30$.

at $z = L/2$ (Figure 9(c)).

In the free-head case, soil inhomogeneity simply redistributes the load along the pile; the maximum load remains close to that of a homogeneous soil for all profiles, whereas the null point moves downwards with increasing soil stiffness below pile mid-depth. Conversely, for the fixed-head energy pile, assuming a homogeneous soil profile with a stiffness equivalent to the actual profile at $z = L/2$ leads to an underestimated axial load, whose magnitude depends on the actual stiffness variation. Consequently, implementing a proper stiffness profile is a crucial task, which is possible by implementing the approach presented herein.

7 EXTENSION TO THERMOMECHANICAL LOADING

The proposed model can be extended to consider the simultaneous application of mechanical and thermal loads. This can be done in a straightforward manner by exploiting the principle of superposition. Recently, Della Corte et al.(2026c) derived a semi-analytical solution for axially loaded floating piles embedded in a generalised inhomogeneous soil profile, which can be simply combined with that proposed in the present study. Thus, the system of algebraic equations for the unknown B_m is modified as follows:

$$\begin{aligned} &A_\mathrm{p} \sum_{m=1}^{N_\mathrm{t}} B_m K_0(s_m) \int_0^h E(z)\, \Phi'_m(z)\, \Phi'_k(z)\, dz \;+\; K_\mathrm{h}\, \Phi_k(0) \sum_{m=1}^{N_\mathrm{t}} B_m K_0(s_m)\, \Phi_m(0) + \\ &2\pi\, B_k\, s_k\, K_1(s_k) \int_0^h G_\mathrm{s}(z)\, \Phi_k^2(z)\, dz = \underbrace{E_\mathrm{p} A_\mathrm{p}\, \alpha \Delta T\, (\Phi_k(L) - \Phi_k(0))}_{\text{thermal}} + \underbrace{P\, \Phi_k(0)}_{\text{mechanical}} \end{aligned} \tag{21}$$

where P is the applied mechanical load. The first term in the right-hand side represents the thermal contribution, while the second accounts for the mechanical one.

The axial force, $N(z)$, resulting from the combined effects of thermal and mechanical loadings, can be conveniently obtained by manipulating the equilibrium equation (14) to account for a different boundary condition at pile head.

The proposed thermo-mechanical solution is verified against some Finite Element analyses available in literature.

Paul and Basu(2026) presented the results of linear elastic analyses of a single floating energy pile embedded in a three-layer soil deposit. The pile is 30 m long with a diameter of 1.2 m and is subjected to an axial mechanical load of $P = 6000$ kN along with a temperature variation of $\Delta T = +30$°C. No restraint is considered at the pile head. The stiffness parameters adopted in the proposed solution for soil and pile were taken directly from the original publication.

Figure 10 shows the axial stress profile obtained with the proposed thermo-mechanical solution, as well as those derived from the numerical analyses; the results using the analytical approach of Paul and Basu(2026) are also reported for comparison. These are split into mechanical, thermal, and combined (mechanical + thermal) profiles. Overall, the comparison confirms that proposed model captures very well the pile response under all the loading conditions considered.

The approach is also verified against the results of tridimensional thermo-hydro-mechanical finite element analyses carried out by Di Donna et al.(2016) in which the soil and pile-soil interface are modelled using a thermoelastic-perfectly plastic constitutive model. After

validating the model using the results of the experimental campaign described above, the authors performed additional analyses in which 3 out of 4 energy piles (namely, EP2, EP3 and EP4) were simultaneously subjected to thermo-mechanical loads. In particular, the applied temperature increase is of 30°C. Note that Di Donna et al.(2016) modelled the foundation as if it were double symmetric. This way, when piles EP2, EP3 and EP4 are heated, their symmetric energy piles are also heated. It follows that K_h has been calibrated ad hoc for the test at hand, including thermal and mechanical pile-to-pile interaction. The soil and pile parameters, as well as the magnitude of the applied mechanical load at the head of each pile, are taken from the original publication. As concern soil stiffness, the same procedure as that adopted for Figure 8 has been used to consider the development of soil nonlinearities. The results of the comparison are reported in Figure 11 in terms of thermo-mechanical stress developed along pile length. The very good agreement detected also for this case confirms the suitability of the proposed solution to serve as a design tool for a preliminary assessment of the performance of energy pile groups in terms of axial loads. As a side comment, it is noted that the temperature variation in the numerical analyses is imposed over one month. This means that the soil is experiencing a certain temperature variation and, thus, its degree of restraint decreases. It follows that, since in the present method the soil is considered at constant temperature, the predictions of the analytical solution result in a larger axial force compared to the FE analyses, as can be detected in the upper part of the pile. Of course, this effect is practically absent in the part of the pile embedded in the very stiff bottom layer.

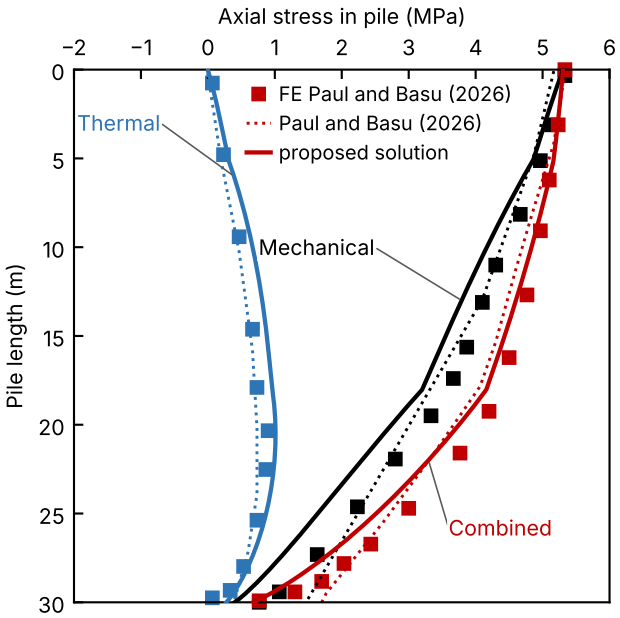


Figure 10: Comparison between the results of finite element and the analytical model of Paul and Basu(2026) and the proposed solution.

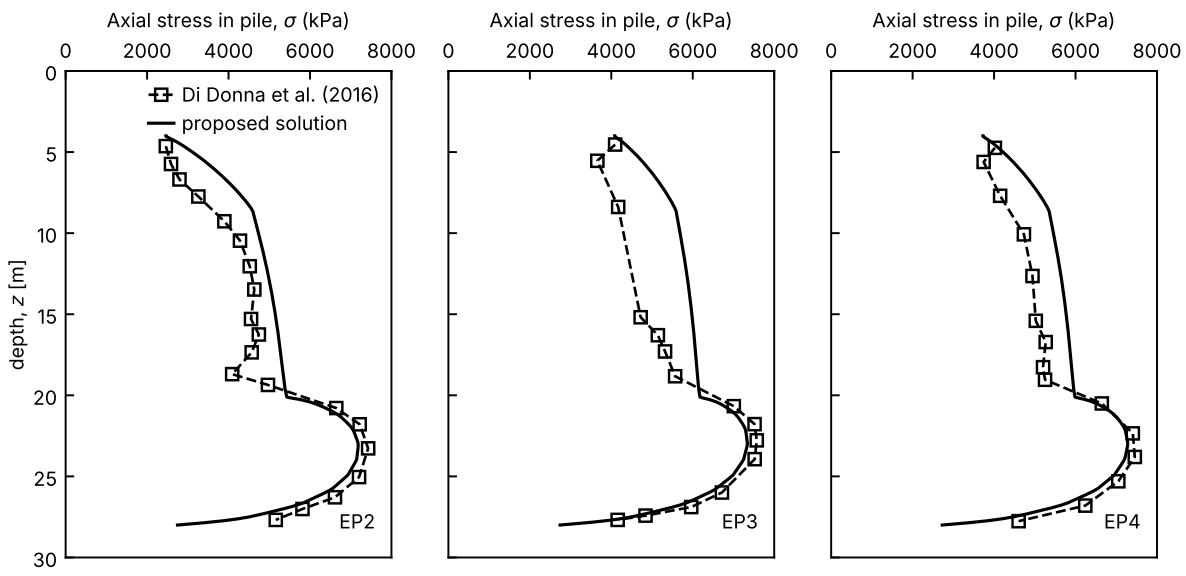


Figure 11: Comparison between the results of the finite element analyses of Di Donna et al.(2016) and the proposed solution.

8 SUMMARY AND CONCLUSIONS

This study presented a novel continuum-based semi-analytical framework for the analysis of floating energy piles embedded in generalised inhomogeneous soils.

The soil is modelled as an approximate Tajimi-type continuum in which only the vertical soil displacement component is considered in the evaluation of the shear and normal stresses. The pile and the soil column beneath its tip (pseudo-pile) are treated as a single axially deforming rod, while the restraint provided by the superstructure or pile-cap system is represented by a concentrated spring at the pile head. Vertical soil inhomogeneity is incorporated through a generalised eigenvalue problem for the evaluation of the soil modes. These modes are approximated by a series expansion in terms of simple trigonometric functions, resulting in a solution expressed as a linear combination of eigenfunctions along the vertical coordinate. Soil temperature is considered to remain constant during pile heating or cooling.

The novelties of this study lie in the development of a unified framework for floating energy piles that accommodates generic soil stiffness profiles and considers pile-head restraint via a dedicated spring while incorporating soil nonlinearity in an simple yet approximate manner. Additionally, the paper introduces a unique semi-analytical approach to determine the thermo-mechanical axial forces under combined mechanical and thermal loading.

The predictive performance of the thermal model was verified against available literature. In particular, analytical solutions, results of some Finite Element analyses as well as some data gathered from field tests are used as benchmarks. These covered several scenarios ranging from homogeneous to layered soil profiles, including free- and fixed-head isolated energy piles, pile groups with simultaneous presence of traditional and thermally-activated piles (thus with partial fixity at head) and development of soil nonlinearity.

The comparisons showed a very satisfactory agreement for all cases. It is worth highlighting that a slight deviation of the proposed approach from the finite-element results is detected in

the vicinity of pile head, especially for homogeneous soils and fixed-head piles. This is due to a localised singularity in the shear stress profile at pile-soil interface, near pile head resulting from the approximate nature of the adopted continuum formulation. Nevertheless, this local effect has limited practical significance, as it does not appreciably affect the overall axial load distribution along the pile.

A parametric analysis was also carried out to investigate the effect of different soil stiffness distributions with depth on the thermally induced axial load. The selected stiffness profiles all match at pile mid-length; moreover, some two-layer distributions were also considered whose average stiffness is equal to that of the homogeneous profile. The results suggested that implementing a proper stiffness profile is important especially for fixed-head piles, since the simple assumption of considering an equivalent homogeneous soil leads to an underestimation of the axial load regardless of the actual distribution of the stiffness. This is simply implementable with the proposed approach.

Finally, the model was extended to consider the simultaneous application of mechanical and thermal loads. The comparison against some Finite Element analyses available in the literature demonstrated good agreement, confirming the validity of the proposed approach.

Given its simplicity and the key feature included to account for pile-head restraint, the proposed approach represents a simple tool for energy pile design, serving as a practical alternative to computationally demanding numerical modelling.

9 Acknowledgements

The research proposed in this paper was supported by KU Leuven through the project "ATHENA" *Analytical & programming efficiency in geoTecHnical ENgineering Applications* (C24E/22/009, KU Leuven Internal Funds), and by University of Campania Luigi Vanvitelli through the project "ALTHEA" *benchmArk soLutions for fundamenTal pilE-soil interAction applications* (No.0081/2023, Visiting Professor 2022-2023 scheme). The authors are grateful for the support.

References

[Amatya et al.(2012)] Amatya, B.L., Soga, K., Bourne-Webb, P.J., Amis, T. & Laloui, L. (2012). *Thermo-mechanical behaviour of energy piles*, Géotechnique, 62(6):503-519, https://doi.org/10.1680/geot.10.P.116.

[Anoyatis and Mylonakis(2012)] Anoyatis, G. & Mylonakis, G. (2012). *Dynamic Winkler modulus for axially loaded piles*, Géotechnique, 62(6):521-536, https://doi.org/10.1680/geot.11.P.052.

[Anoyatis(2013)] Anoyatis, G. (2013). *Contribution to Kinematic and Inertial Analysis of Piles by Analytical and Experimental Methods*, PhD thesis, Civil Engineering Department, University of Patras, Patras, Greece.

[Anoyatis et al.(2019)] Anoyatis, G., Mylonakis, G. & Tsikas, A. (2019). *An analytical continuum model for axially loaded end bearing piles in inhomogeneous soil*, International Journal for Numerical and Analytical Methods in Geomechanics, 43(6):1162-1183, https://doi.org/10.1002/nag.2886.

[Anoyatis et al.(2023)] Anoyatis, G., François, S., Orakci, O. & Tsikas, A. (2023). *Soil-pile interaction in vertical vibration in inhomogeneous soils*, Earthquake Engineering & Structural Dynamics, 52(14):4582-4601, https://doi.org/10.1002/eqe.3968.

[Bourne-Webb et al.(2009)] Bourne-Webb, P.J., Amatya, B., Soga, K., Amis, T., Davidson, C. & Payne, P. (2009). *Energy pile test at Lambeth College, London: geotechnical and thermodynamic aspects of pile response to heat cycles*, Géotechnique, 59(3):237-248, https://doi.org/10.1680/geot.2009.59.3.237.

[Brandl(2006)] Brandl, H. (2006). *Energy foundations and other thermo-active ground structures*, Géotechnique, 56(2):81-122, https://doi.org/10.1680/geot.2006.56.2.81.

[de Silva et al.(2025)] de Silva, F., Iodice, C. & Russo, G. (2025). *Time-dependent interaction coefficients to quantify the settlement of energy pile groups*, Canadian Geotechnical Journal, 62:1-16, https://doi.org/10.1139/cgj-2024-0576.

[Della Corte et al.(2025)] Della Corte, A., Letizia, N., Tsikas, A., François, S. & Anoyatis, G. (2025). *Dynamic soil pressures on rigid vertical walls in presence of generalized inhomogeneous soils*, Earthquake Engineering & Structural Dynamics, 54(5):1342-1360, https://doi.org/10.1002/eqe.4306.

[Della Corte et al.(2026a)] Della Corte, A., Iodice, C., Tsikas, A., François, S. & Anoyatis, G. (2026a). *An analytical approach to pile-to-pile interaction for end-bearing piles*, Géotechnique, 76(2):247-258, https://doi.org/10.1680/jgeot.24.01159.

[Della Corte et al.(2026b)] Della Corte, A., François, S., Tsikas, A., Vankeirsbilck, J., Boydens, J. & Anoyatis, G. (2026b). *An analytical model for axial kinematic and inertial loading of single end-bearing piles embedded in generalised inhomogeneous soils*, Soil Dynamics and Earthquake Engineering, 200:109701, https://doi.org/10.1016/j.soildyn.2025.109701.

[Della Corte et al.(2026c)] Della Corte, A., François, S., Iodice, C., Tsikas, A. & Anoyatis, G. (2026c). *An analytical model for axially-loaded floating piles in continuously inhomogeneous and two-layer soils*, International Journal for Numerical and Analytical Methods in Geomechanics, 50(13):4981-4993, https://doi.org/10.1002/nag.70374.

[Della Corte et al.(2026d)] Della Corte, A., Iodice, C., François, S., Tsikas, A. & Anoyatis, G. (2026d). *Continuum analytical models for the ultimate limit state design of floating energy piles*, Proceedings of GEOTEC HANOI 2026, Hanoi, Vietnam, November 26-27, 2026, accepted for publication.

[Di Donna et al.(2016)] Di Donna, A., Loria, A.F.R. & Laloui, L. (2016). *Numerical study of the response of a group of energy piles under different combinations of thermo-mechanical loads*, Computers and Geotechnics, 72:126-142, https://doi.org/10.1016/j.compgeo.2015.11.010.

[Di Laora & Rovithis(2015)] Di Laora, R. & Rovithis, E. (2015). *Kinematic bending of fixed-head piles in nonhomogeneous soil*, Journal of Geotechnical and Geoenvironmental Engineering, 141(4):04014126, https://doi.org/10.1061/(ASCE)GT.1943-5606.0001270.

[Huang et al.(2025)] Huang, L., Ding, Z. & Song, C. (2025). *A novel three-dimensional analytical model for the thermomechanical responses of energy piles and the surrounding soil based on thermoelastic theory*, International Journal for Numerical and Analytical Methods in Geomechanics, 49:2749-2762, https://doi.org/10.1002/nag.4010.

[Iodice et al.(2020)] Iodice, C., Di Laora, R. & Mandolini, A. (2020). *Analytical solutions for ultimate limit state design of thermal piles*, Journal of Geotechnical and Geoenvironmental Engineering, 146(5):04020016, https://doi.org/10.1061/(ASCE)GT.1943-5606.0002204.

[Iodice et al.(2020b)] Iodice, C., Di Laora, R. & Mandolini, A. (2020). *Finite element analyses of energy piles using different constitutive models*, E3S Web of Conferences, 205:05013, https://doi.org/10.1051/e3sconf/202020505013.

[Iodice et al.(2023)] Iodice, C., Di Laora, R. & Mandolini, A. (2023). *A practical method to design thermally stressed piles*, Géotechnique, 73(1):30-43, https://doi.org/10.1680/jgeot.20.P.231.

[Iodice & Anoyatis(2024)] Iodice, C. & Anoyatis, G. (2024). *Continuum analytical models for the ultimate limit state design of energy piles*, In: Duc Long, P. & Dung, N.T. (eds), *Proceedings of the 5th International Conference on Geotechnics for Sustainable Infrastructure Development. GEOTEC 2023*, Lecture Notes in Civil Engineering, 395:395-409, Springer, Singapore.

[Knellwolf et al.(2011)] Knellwolf, C., Peron, H. & Laloui, L. (2011). *Geotechnical analysis of heat exchanger piles*, Journal of Geotechnical and Geoenvironmental Engineering, 137(10):890-902, https://doi.org/10.1061/(ASCE)GT.1943-5606.0000513.

[Liu and Liu(2024)] Liu, H. & Liu, Q. (2024). *Static response of vertically loaded pile in inhomogeneous soil*, Géotechnique Letters, 14(2):71-77, https://doi.org/10.1680/jgele.23.00100.

[Lyu et al.(2026)] Lyu, W., Li, Y., Xia, M., Wang, Z., Zhao, X. & Huang, S. (2026). *Analytical solutions for thermomechanical coupling of semifloating energy piles in multilayer soils*, International Journal of Geomechanics, 26(6):04026102, https://doi.org/10.1061/IJGNAI.GMENG-12819.

[Mimouni and Laloui(2015)] Mimouni, T. and Laloui, L. (2015). *Behaviour of a group of energy piles*, Can. Geotech. J., 52(12):1913-1929, https://doi.org/10.1139/cgj-2014-0403.

[Mylonakis(2001)] Mylonakis, G. (2001). *Winkler modulus for axially loaded piles*, Géotechnique, 51(5):455-461, https://doi.org/10.1680/geot.2001.51.5.455.

[Najma and Sharma(2021)] Najma, A. & Sharma, J. (2021). *Incremental load transfer analysis of an energy pile under arbitrary mechanical and thermal loads*, Geomechanics for Energy and the Environment, 28:100243, https://doi.org/10.1016/j.gete.2021.100243.

[Nogami & Novák(1976)] Nogami, T. & Novák, M. (1976). *Soil-pile interaction in vertical vibration*, Earthquake Engineering & Structural Dynamics, 4(3):277-293, https://doi.org/10.1002/eqe.4290040308.

[Olia & Perić(2021)] Olia, A.S.R. & Perić, D. (2021). *Thermomechanical Soil-Structure Interaction in Single Energy Piles Exhibiting Reversible Interface Behavior*, International Journal of Geomechanics, 21(5):04021065, https://doi.org/10.1061/(ASCE)GM.1943-5622.0002014.

[Paul and Basu(2026)] Paul, A. & Basu, D. (2026). *Thermomechanical framework for settlement calculation of geothermal energy piles in multilayered soil*, International Journal of Geomechanics, 26(10):04026192, https://doi.org/10.1061/IJGNAI.GMENG-13273.

[Perić et al.(2020)] Perić, D., Cossel, A.E. & Sarna, S.A. (2020). *Analytical Solutions for Thermomechanical Soil-Structure Interaction in End-Bearing Energy Piles*, Journal of Geotechnical and Geoenvironmental Engineering, 146(7):04020047, https://doi.org/10.1061/(ASCE)GT.1943-5606.0002269.

[Randolph and Wroth(1978)] Randolph, M.F. & Wroth, C.P. (1978). *Analysis of vertical deformation of vertically loaded piles*, Journal of Geotechnical and Geoenvironmental Engineering, 104(12):1465-1488, https://doi.org/10.1061/AJGEB6.0000729.

[Rotta Loria and Laloui(2016)] Rotta Loria, A.F. & Laloui, L. (2016). *The interaction factor method for energy pile groups*, Computers and Geotechnics, 80:121-137, https://doi.org/10.1016/j.compgeo.2016.07.002.

[Rotta Loria and Laloui(2018)] Rotta Loria, A. F. and Laloui, L. (2018). *Group action effects caused by various operating energy piles*, Géotechnique, 68(9):834-841, https://doi.org/10.1680/jgeot.17.P.213.

[Salgado et al.(2013)] Salgado, R., Seo, H. & Prezzi, M. (2013). *Variational elastic solution for axially loaded piles in multilayered soil*, International Journal for Numerical and Analytical Methods in Geomechanics, 37(4):423-440, https://doi.org/10.1002/nag.1110.

[Tajimi(1969)] Tajimi, H. (1969). *Dynamic analysis of a structure embedded in an elastic stratum*, Proceedings of the 4th World Conference on Earthquake Engineering, 3:53-69.

[Vardanega and Bolton(2011)] Vardanega, P.J. & Bolton, M.D. (2011). *Predicting shear strength mobilization of London clay*, Proc., 15th European Conf. on Soil Mechanics and Geotechnical Engineering, 1:487-492, IOS Press, Amsterdam, Netherlands.

[Veletsos and Younan(1994)] Veletsos, A.S. & Younan, A.H. (1994). *Dynamic soil pressures on rigid vertical walls*, Earthquake Engineering & Structural Dynamics, 23(3):275-301, https://doi.org/10.1002/eqe.4290230305.